



Classifying Core Collapse Supernova Remnants by Their Morphology as Shaped by the Last Exploding Jets

Noam Soker

Department of Physics, Technion, Haifa, 3200003, Israel; soker@physics.technion.ac.il

Received 2023 August 3; revised 2023 August 17; accepted 2023 August 24; published 2023 October 9

Abstract

Under the assumption that jets explode all core collapse supernovae (CCSNe), I classify 14 CCSN remnants (CCSNRs) into five groups according to their morphology as shaped by jets, and attribute the classes to the specific angular momentum of the pre-collapse core. *Point-symmetry* (one CCSNR): According to the jittering jets explosion mechanism (JJEM) when the pre-collapse core rotates very slowly, the newly born neutron star (NS) launches tens of jet-pairs in all directions. The last several jet-pairs might leave an imprint of several pairs of “ears,” i.e., a point-symmetric morphology. *One pair of ears* (eight CCSNRs): More rapidly rotating cores might force the last pair of jets to be long-lived and shape one pair of jet-inflated ears that dominates the morphology. *S-shaped* (one CCSNR): The accretion disk might precess, leading to an S-shaped morphology. *Barrel-shaped* (three CCSNRs): Even more rapidly rotating pre-collapse cores might result in a final energetic pair of jets that clear the region along the axis of the pre-collapse core rotation and form a barrel-shaped morphology. *Elongated* (one CCSNR): A very rapidly rotating pre-collapse core forces all jets to be along the same axis such that the jets are inefficient in expelling mass from the equatorial plane and the long-lasting accretion process turns the NS into a black hole. The two new results of this study are the classification of CCSNRs into five classes based on jet-shaped morphological features, and the attribution of the morphological classes mainly to the pre-collapse core rotation in the frame of the JJEM.

Key words: stars: massive – stars: neutron – stars: black holes – (stars:) supernovae: general – ISM: supernova remnants – stars: jets

1. Introduction

There is no consensus on the explosion mechanism of core collapse supernovae (CCSNe). There are two competing theoretical explosion mechanisms that are based on the gravitational energy that the formation process of the newly born neutron star (NS) or black hole (BH) releases as the core of the CCSN progenitor collapses. These mechanisms are the delayed neutrino explosion mechanism (Bethe & Wilson 1985, followed by hundreds of studies since then, e.g., Heger et al. 2003; Janka 2012; Nordhaus et al. 2012; Müller et al. 2019; Burrows & Vartanyan 2021; Fujibayashi et al. 2021; Fryer et al. 2022; Baccioli et al. 2022; Nakamura et al. 2022; Olejak et al. 2022), and the jittering jets explosion mechanism (JJEM; Soker 2010, with a limited number of studies that followed Papish & Soker 2011; Gilkis & Soker 2015; Quataert et al. 2019; Soker 2020; Shishkin & Soker 2021; Antoni & Quataert 2023; Soker 2022a; Soker 2023).

According to the JJEM, intermittent accretion disks (or belts; e.g., Schreier & Soker 2016) with stochastically varying angular momentum axes launch pairs of jets that explode the star. Pre-collapse stochastic core convection motion (e.g., Soker 2010; Papish & Soker 2014b; Gilkis & Soker 2015;

Soker 2019; Shishkin & Soker 2022; Soker 2022a, 2022b; in some cases envelope convection motion can supply these seed perturbations, e.g., Quataert et al. 2019; Antoni & Quataert 2023) serves as seed angular momentum perturbations. Instabilities between the newly born NS and the stalled shock at $\simeq 100$ km from the NS amplify these seed perturbations to sufficiently large specific angular momentum fluctuations to form the intermittent accretion disks (e.g., Shishkin & Soker 2021). In case of core rotation, the stochastic angular momentum variations are around the angular momentum axis of the pre-collapse core (e.g., Soker 2023).

There are some fundamental differences between the JJEM and many papers that study jet-driven explosions that operate only for rapidly rotating pre-collapse cores and therefore the jets that the newly born NS or BH launch have a fixed axis (e.g., Khokhlov et al. 1999; Aloy et al. 2000; MacFadyen et al. 2001; Maeda et al. 2012; López-Cámara et al. 2013; Bromberg & Tchekhovskoy 2016; Nishimura et al. 2017; Wang et al. 2019; Grimmer et al. 2021; Perley et al. 2021; Gottlieb et al. 2022; Obergaulinger & Reichert 2023; Urrutia et al. 2023). These differences are as follows (e.g., Soker 2022c). (1) As explained above, the JJEM operates even when the pre-collapse core does not rotate. (2) The JJEM asserts that jets explode

most, and possibly all, CCSNe. (3) This implies that there are no failed CCSNe in the frame of the JJEM. All massive stars explode, even when a BH is formed. (4) The JJEM operates in a jet negative feedback mechanism. Namely, when the jets manage to explode the star, accretion stops (with some delay time). This accounts for explosion energies that are several times the binding energy of the ejected mass.

There might be \approx few – 30 jet-launching episodes during the entire explosion process with the following properties (Papish & Soker 2014a). The jet launching velocities are $\approx 10^5 \text{ km s}^{-1}$ (neutrino observations limit the jets in most cases to be non-relativistic, e.g., Guetta et al. 2020). The explosion time might be $\approx 1\text{--}10$ s, where each individual jet-launching episode lasts for $\approx 0.01\text{--}0.1$ s, besides probably the last jet-launching episode that might in some cases be much longer, as I propose in this study. The two jets in each jet-launching episode carry a mass of $\approx 10^{-3} M_{\odot}$. During the explosion process the newly born NS accretes a mass of $\approx 0.1 M_{\odot}$ through intermittent accretion disks, i.e., each accretion disk of an episode has a mass of $\approx 10^{-2} M_{\odot}$. These properties can vary a lot from one CCSN to another because they depend on the convection motion in the pre-collapse core, its angular momentum and the binding energy of the ejecta.

As far as the basic outcomes of the explosions, e.g., nucleosynthesis and lightcurves, are concerned, the JJEM is similar to the neutrino driven-mechanism. The JJEM includes also heating by neutrinos as a boosting process (Soker 2022b). The differences include the morphology of the ejecta and the aspect that the JJEM can explain also very energetic CCSNe. This study deals with the morphology that the late jets imprint on the ejecta. Early jets are choked inside the core, deposit their energy in the core and explode it. Instabilities in the JJEM develop similarly, but not identically, to those in the neutrino-driven explosion mechanism (for the latter see, e.g., Wongwathanarat et al. 2015, 2017; Burrows & Vartanyan 2021; Vartanyan et al. 2022). The jets are expected to introduce a point-symmetrical morphological component to the instabilities and mixing of isotopes. By point-symmetry I refer to a structure where for each structural feature there is a counterpart on the other side of the center. Because of the highly non-spherical explosion process, the counter structural feature can have a different small-scale structure, a different brightness and be at a different distance from the center. The best example is the supernova remnant (SNR) 0540-69.3 that I study in Section 2.1.2, which possesses point-symmetry in its inner regions (Soker 2022a).

In this study, however, I focus on late jets, namely, jets that the newly born NS or BH launch after the earlier jets explode the core. I examine the morphological features that such jets imprint on the outer regions of the ejecta as observed in CCSN remnants (CCSNRs). In Section 2, I classify 14 SNRs into five classes. In Section 3, I suggest that the main, but not sole, property that determines the class of an SNR is the pre-collapse

core angular momentum. This proposed explanation, and actually this entire paper, is largely motivated by my recently proposed explanation for the NS to BH mass gap in the frame of the JJEM (Soker 2023). I summarize this study in Section 4.

2. Classification of SNRs

I classify 14 CCSNRs into five classes. Many other CCSNRs morphologies are too “messy” and do not allow classification into one of these classes, e.g., VRO 42.05.01 (G166.0+4.3; for an image see, e.g., Xiao et al. 2022). I describe each class in a separate subsection and in the same order as the classes appear in Table 1. The first row of Table 1 lists the five classes and the lower rows list the CCSNRs in each class. The second row refers to my suggestion as to the main (but not sole) effect that determines the morphological properties of the last jets to be launched in the explosion process according to the JJEM (Section 3). I assume that the main shaping of the morphology is by jets and not by other processes, such as the magnetic field of the interstellar medium (ISM, e.g., Wu & Zhang 2019; Velázquez et al. 2023). The variable j_p is the pre-collapse average specific angular momentum of the core material that the newly born NS accretes as it launches jets; “p” stands for pre-collapse rotation which has a fixed direction. The variable j_f is the amplitude of the fluctuations in the specific angular momentum of the material that the NS accretes due to the velocity fluctuations of the pre-collapse convective zone. The amplitude is after instabilities amplify the perturbations. The direction of this angular momentum component varies stochastically; “f” stands for fluctuating directions.

2.1. Point-symmetry

Point-symmetry morphological features in CCSNRs are clear predictions of the JJEM. Therefore, the two CCSNRs that I study in this section strongly support the JJEM.

2.1.1. The Vela SNR

The best example of an SNR that contains point-symmetric morphological features is the SNR Vela that I present in Figure 1. This is a ROSAT X-ray image (Aschenbach et al. 1995) that is based on Figure 1 from Sapienza et al. (2021). The white AG-line is from their figure and was already drawn by García et al. (2017). The labeling of the clumps is also from Sapienza et al. (2021), where clumps A-F were identified by Aschenbach et al. (1995). The high Si abundance of clump A (Katsuda & Tsunemi 2006) and of clumps G and K (García et al. 2017) indicates that, as in Cassiopeia A (Section 2.2), these clumps originate from deep inside the core of the progenitor. Sapienza et al. (2021) convincingly argue that clumps K and G are indeed counter to clump A, and represent jet-like structure from the explosion process. Katsuda & Tsunemi (2005) analyze clump D and find it to be

Table 1
The Classification of CCSNRs into Five Classes According to the Last Jets to be Launched in the Explosion

Point-Symmetry	One pair of ears	S-shaped	Barrel-shaped	Elongated
$j_p \lesssim 0.01j_f$	$0.01j_f \lesssim j_p \lesssim 0.1j_f$	$0.01j_f \lesssim j_p \lesssim 0.1j_f$	$j_p \approx 0.1j_f - 0.3j_f$	$j_p \gtrsim j_f$
Vela [1] (0540-69.3) [#]	0540-69.3 [2]; Cassiopeia A [3]; 3C58 [3]; S147 [3]; G290.1-0.8 [4]; N49B [5]; Puppis A [5]; Crab Nebula [5]	W4 [6]	RCW 103[7] G292.0+1.8 [8] G309.2-00.6 [9]	W50 [10]

Note. The second row lists the relation between the pre-collapse average specific angular momentum of the core j_p , and the magnitude of the stochastic fluctuations in the specific angular momentum of the mass that the newly born NS or BH accretes, j_f (see Section 3). Comments: # The inner structure of SNR 0540-69.3 is point symmetric. However, in this study I focus on the last jets to be launched, and therefore I include this SNR in the one-pair class (Figure 2). Small numbers inside square parentheses are the figures where I present the CCSNRs.

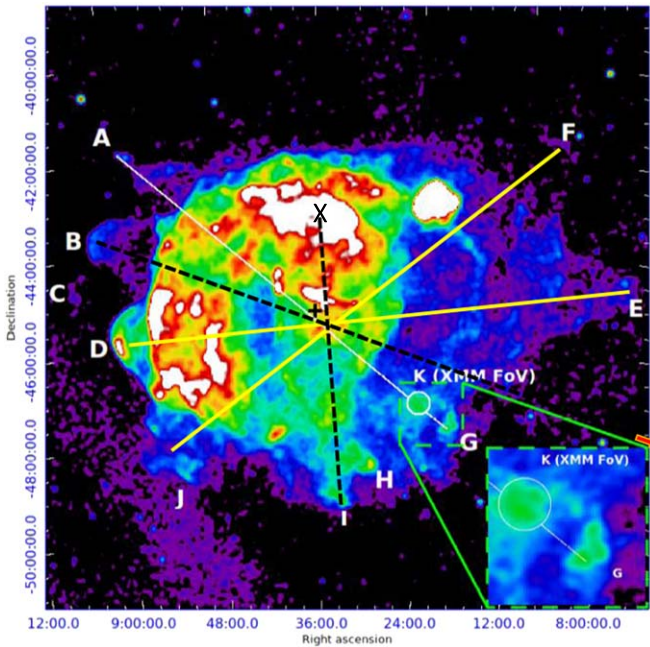


Figure 1. ROSAT X-ray image of SNR Vela (Aschenbach et al. 1995), based on Figure 1 from Sapienza et al. (2021). The white AG-line and the labeling of the clumps are from their figure (clumps A-F are from Aschenbach et al. 1995). I added the thick-yellow DE-line and the FJ-line. I also added two dashed-black lines that connect clumps to my assumed counter jets.

overabundant in ONeMg, which suggests that its origin is from near the center of the remnant, as also suggested by Sankrit et al. (2003). Grichener & Soker (2017) analyze the ears D and E to be the only ears in SNR Vela, and estimate that the combined energy of the jets that inflated ears D and E is only $\approx 1\%$ of the Vela explosion energy. This is the lowest value among the eight SNRs with ears that they analyze.

I added to Figure 1 the thick-yellow DE-line and the FJ-line, each connecting two previously identified clumps. I here claim that each of the clump pairs AG, DE and FJ was inflated by one late jet-launching episode during the explosion of Vela.

Furthermore, I speculate that the jet that ejected clump B had a counter jet. However, because of the lower density ejecta in the counter-jet-B direction (southwest) this clump moved to larger distances than any other clump, and it is below the detection limit. I mark this assumption by a red-orange arrow on the right edge of the figure, and connect it with a dashed-black line to clump B. In the case of clump I, which I take also to have been formed by a jet, I suggest that the counter-clump (s) is immersed in the large white area in the north. I mark it with a black “X.” Indeed, Miceli et al. (2008) identified several shrapnels in that region. Miceli et al. (2008) find that some of these shrapnels have enhanced Ne and Mg abundances, implying they are ejecta from inner stellar zones. In the JJEM, the different compositions of different clumps (shrapnels) suggest that the jets interacted with different layers of the core. The final composition depends on the exact time the jet was launched and how deep it penetrated through inner layers of the core.

Overall, in the frame of the JJEM I identify five late jet-launching episodes. There might be more but such that the clumps are projected on the main ejecta of the SNR and therefore are not identified as fast-moving clumps. If the energy of these jets is similar to the energy of the jets that inflated ears D and E as Grichener & Soker (2017) estimated, then the total energy of the late jets is $\approx 5\%$ of the explosion energy of Vela. This energy is close to the energy of late jets of CCSNRs that have only one late jet-launching episode (Section 2.2).

2.1.2. SNR 0540-69.3

Another SNR with a point-symmetric morphological component is SNR 0540-69.3. I analyzed its point-symmetric morphology (Soker 2022a) as revealed by the detailed observations of Larsson et al. (2021). I present this SNR in Figure 2. Five panels are Very Large Telescope (VLT)/MUSE velocity maps that Larsson et al. (2021) present and which reveal the point-symmetric structure in that plane. This plane is along the line of sight and through the center of the SNR, more or less along the yellow double-headed arrow in the lower-

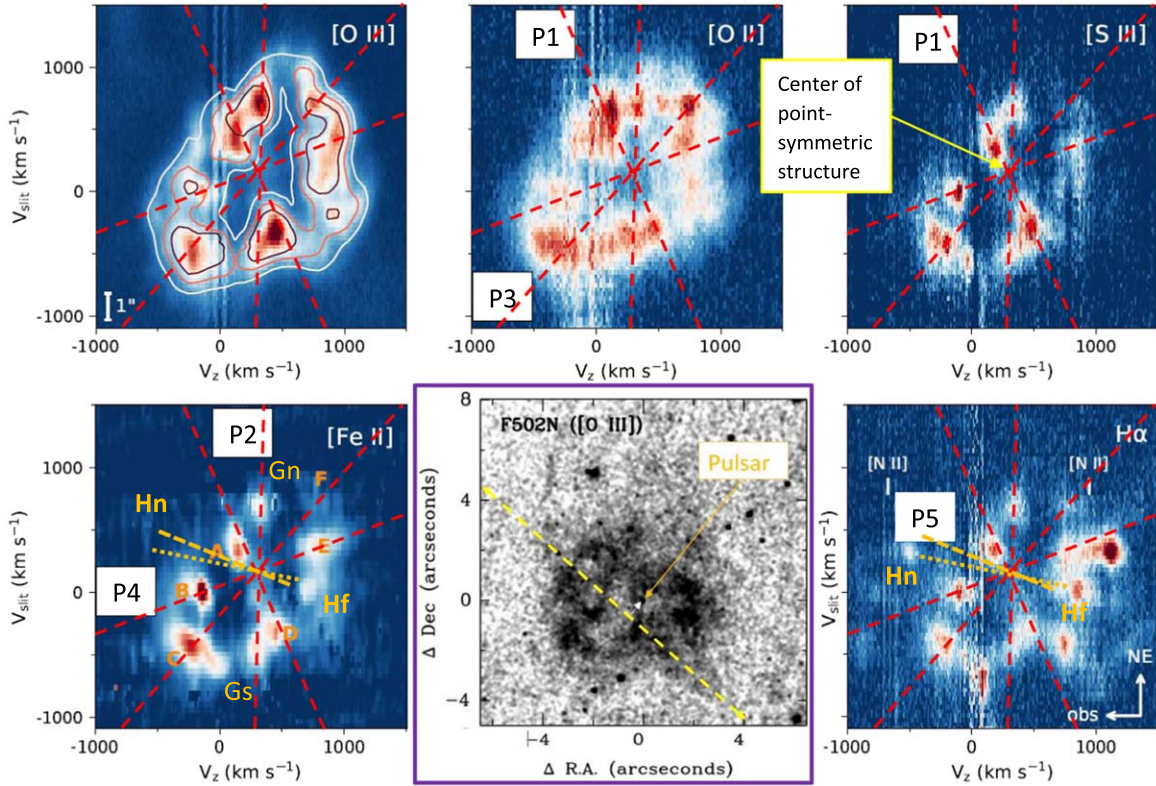


Figure 2. Five panels of two-dimensional velocity maps of SNR 0540-69.3 based on Figure 4 by Larsson et al. (2021). The velocities are along a slit that is more or less along the dashed yellow line in the lower-middle panel: v_{slit} is the velocity along the slit (positive to the northeast), while v_z is the velocity along the line of sight. The lower-middle panel is an HST image from Morse et al. (2006) to which I added the yellow double-headed arrow. The four dashed-red lines in the five panels that connect opposite clumps are from Soker (2022a), where more details can be found. Clumps A to F are marked by Larsson et al. (2021) and clumps Gn and Gs by Soker (2022a). I here added the dashed-orange and dotted-orange lines in the two lower velocity maps to indicate another pair, clump Hf and its counter clump Hn. The pulsar is at $v_{\text{slit}} = 0$ in these panels.

middle panel of Figure 2. This panel is a Hubble Space Telescope (HST) observation from Morse et al. (2006).

There are four pairs of two opposite clumps in the velocity maps that compose the point-symmetric structure of SNR 0540-69.3. Unlike the case of SNR Vela where the clumps are at the outskirts of the SNR, in SNR 0540-69.3 the point-symmetric clumps appear in the center of the ejecta (as is evident by their relatively low expansion velocity). I argued in Soker (2022a) that two to four pairs of jittering jets shaped the inner ejecta in this plane. Here I add another possible pair of clumps as the lines P5 in the lower panels indicate. The clump Hf appears in both the [Fe II] map (lower-left panel) and in the $H\alpha$ map (lower-right panel) at about the same place. The much fainter counter-clump Hn is not exactly at the same place in the two velocity maps. So I draw two lines, the dashed-orange one represents the pair in the [Fe II] map and the dotted-orange one signifies the pair in the $H\alpha$ velocity map. Overall, I here claim there are five pairs that form the point-symmetric structure in the velocity maps.

The lower-middle panel presents a hollowed central region (a faint strip) that connects two ears, with the southwest being much longer. The yellow double-headed arrow in the lower-middle panel is along this hollowed region. As the yellow double-headed arrow is more or less the direction of the slit that Larsson et al. (2021) use for the velocity maps, the pair of ears, which is part of the point-symmetric structure, is in the same plane as the five pairs of clumps that the velocity maps reveal. In Soker (2022a) I pointed out that the similarity of the point-symmetric structure of SNR 0540-69.3 with some planetary nebulae, e.g., He2-138 (PN G320.1-09.6; image in Sahai & Trauger 1998) and M1-37 (PN G002.6-03.4; image in Sahai 2000), strongly suggests shaping by jets.

The SNR 0540-69.3 can be classified as point-symmetric with a hollowed-cylinder (barrel-like) structure (more details are in Soker 2022a). Without the detailed analysis by Larsson et al. (2021), and based only on the HST observations by Morse et al. (2006), this SNR would have been classified as having one-pair of ears. However, while in the SNR Vela the point-symmetric structure is in the outer parts of the ejecta, the

velocity maps of SNR 0540-69.3 reveal a point-symmetric structure in the inner parts of the ejecta. It seems that this inner structure was shaped by the jets that exploded the star. Namely, in addition to instabilities in the explosion process (Section 1), jets also shape the inner ejecta. The jets can play a role in mixing elements in the ejecta of CCSNe.

However, as far as late jets are concerned, I classify SNR 0540-69.3 in the one-pair of ears morphological class.

2.2. One Pair of Ears

CCSNRs which have one pair of ears that dominate their morphology is the largest class. An ear is defined as a protrusion from the main ejecta (nebula) that is fainter than the general nebula, and has a cross section that monotonically decreases from its base on the main nebula to its tip. In most cases the two ears in a pair are neither equal in terms of their size and intensity to each other, nor in terms of their distance from the center. The asymmetry is another manifestation of the asymmetrical explosion process of CCSNe that involves instabilities as well as large scale asymmetries. Another prominent manifestation of the asymmetrical explosion is NS natal kick (which I do not study here).

Grichener & Soker (2017) and Bear et al. (2017) study many of these CCSNRs and estimated the extra energy of the jets that inflated the pair of bubbles. These studies find that the extra energy varies between different CCSNRs, from being $\simeq 1\%$ to $\simeq 30\%$ of the total explosion energy. I here examine only the morphology. In Figures 3–5 I present seven images, mostly from Grichener & Soker (2017) who marked with double-headed arrows the base and middle of the ears.

One of the best examples of the one-pair class is S147 that I also present in Figure 3 (for a recent study of this SNR see, e.g., Ren et al. 2018). The two other SNRs in Figure 3 and the one in Figure 4 have one ear much larger than the other. Figure 5 presents three SNRs with ears that do not protrude much from the main ejecta (nebula).

2.3. S-shaped Morphology

This class includes only the SNR W44 that I present in Figure 6 taken from the Chandra gallery with lines from Grichener & Soker (2017). The S-shaped morphology is most likely due to precession of the jets around a fixed axis. The two ears are neither symmetric with respect to the pulsar nor with respect to the main shell.

The morphology of W44 is of one pair of ears that is arranged in an S-shape. It can as well belong to the one-pair class. However, the very likely cause of an S-shape is jet-precession. Namely, it was the accretion disk that launched the last jets that performed precession while launching the jets. This suggests, in the frame of the JJEM, a non-negligible pre-collapse core rotation as I discuss in Section 3.

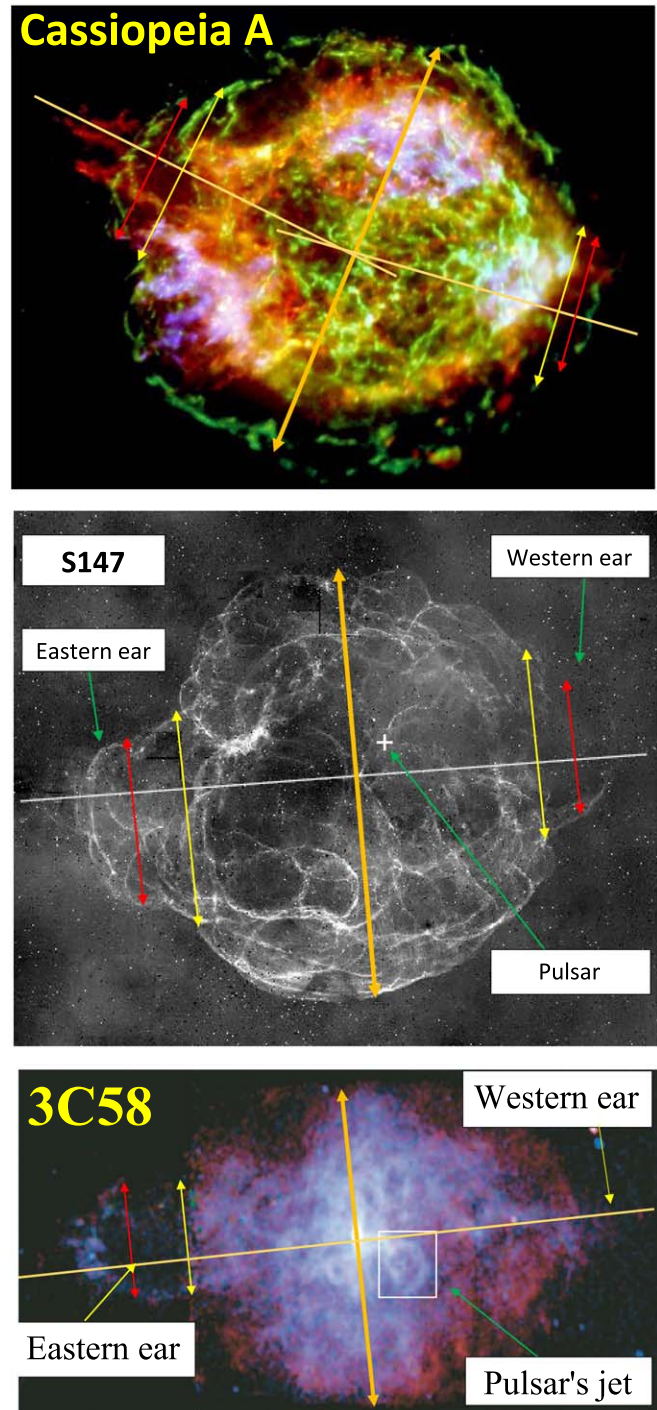


Figure 3. Images of three SNRs where one pair of ears dominates the outer morphology, and where at least one ear is large and prominent. Upper three images: The identifications of the ears and the double-headed arrow marks of the base of an ear at the main ejecta and of the center of an ear are from Grichener & Soker (2017). The sources of the images are as follows. *Cassiopeia A*: An X-ray image taken from the Chandra gallery (based on Hwang et al. 2004). *S147*: An $H\alpha$ image from Gvaramadze (2006) who reproduced an image from Drew et al. (2005). *3C58*: Chandra/ACIS image from the Chandra Gallery based on Slane et al. (2004); colors represent energy bands.

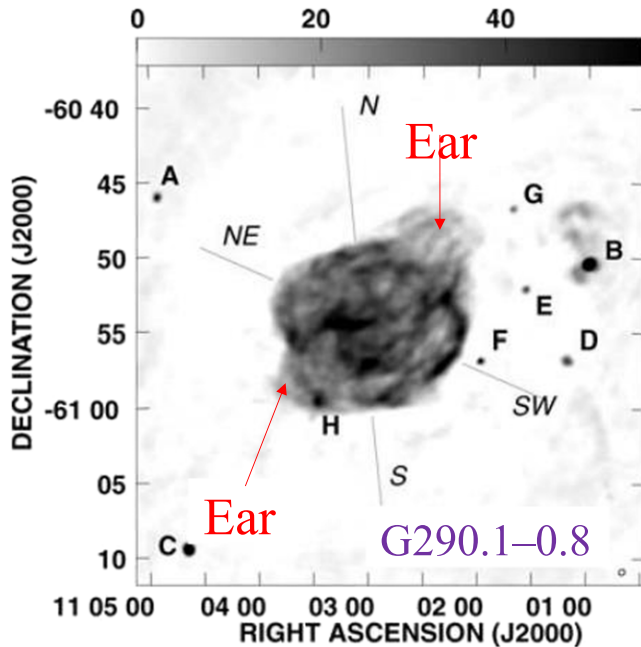


Figure 4. Radio continuum image at 1384 MHz of SNR G290.1–0.8 that morphologically belongs to SNRs in Figure 3; From Reynoso et al. (2006) to which I added the identification of ears.

2.4. Barrel-shaped SNRs

A barrel-shaped morphology refers to a general axisymmetrical structure with a central region along the symmetry axis that is much fainter than the sides. The two ends on the symmetry axis are trimmed. Its hollowed structure appears in observations as two opposite bright arcs with a faint (hollowed) region between them. The best example of a barrel-shaped SNR is RCW 103 that I present in Figure 7. I take this X-ray image (Rea et al. 2016) from Bear et al. (2017) who proposed the shaping of RCW 103 by two jets at the final phase of the explosion. They based the jet-shaping model on the morphological similarities of RCW 103 with several barrel-shaped planetary nebulae that are observed to be shaped by jets. The unequal structure of the two arcs, which are the projection of the barrel-structure on the plane of the sky, can result from a density gradient in the ISM (e.g., Lu et al. 2021) or from asymmetrical explosion.

The case of SNR G292.0+1.8 is subtle as it shows both a barrel-shaped morphology and two opposite ears. In Figure 8 I present an image from Bear et al. (2017) where more details can be found. The visible images of $H\alpha$ (upper-right panel) and [O III] (lower-left panel) display the barrel-shaped morphology. Bear et al. (2017) indicate the symmetry axis of the barrel-shaped morphology by the double-headed pink line in the $H\alpha$ image. The X-ray images, on the other hand, present two very small opposite ears that Bear et al. (2017) mark and analyze. Because the two opposite arcs in the $H\alpha$ image display a very

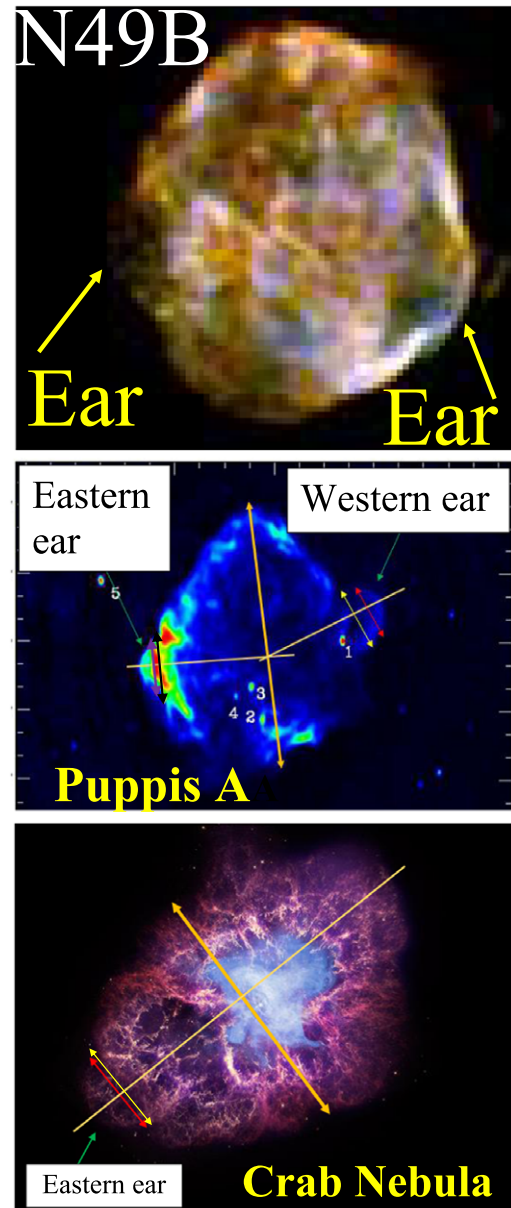


Figure 5. Images of three SNRs with one pair of ears that does not protrude much from the main ejecta. Sources of marks in the two lower panels are from Grichener & Soker (2017). The sources of the images are as follows. *N49B*: An X-ray image from the Chandra gallery based on Park et al. (2003). *Puppis A*: The radio continuum emission at 1.4 GHz; published by Reynoso & Walsh (2015) and reproduced by Reynoso et al. (2017). *Crab Nebula*: A composite image of X-ray (blue; Seward et al. 2006), optical (red-yellow; Hester 2008), and infrared (Purple; NASA/JPL-Caltech/Univ).

prominent barrel-shaped morphology instead of two small ears, I classified it as a barrel-shaped SNR.

SNR G309.2-00.6 that I present in Figure 9 with marks from Grichener & Soker (2017) also presents a complicated case. It has two prominent ears as marked on the figure. However, in

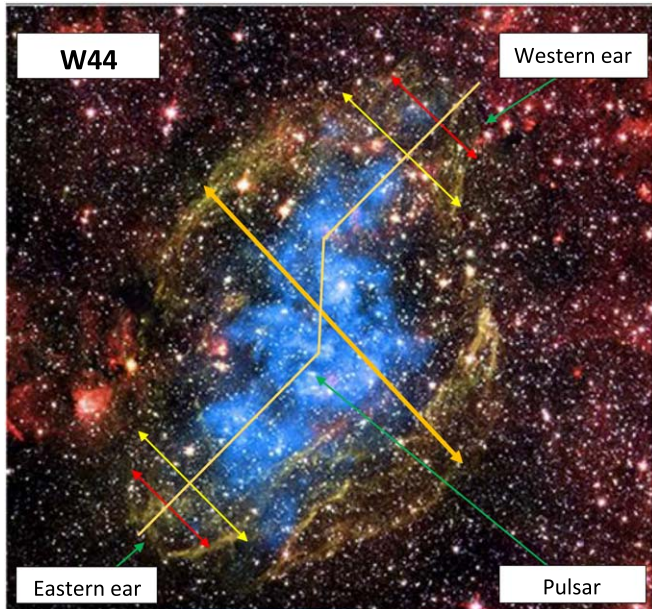


Figure 6. A composite image of SNR W44 taken from the Chandra gallery with marks from Grichener & Soker (2017). The cyan color represents X-ray (based on Shelton et al. 2004). The red, blue, and green signify infrared emission (based on NASA/JPL-Caltech). This SNR has a prominent S-shaped morphology.

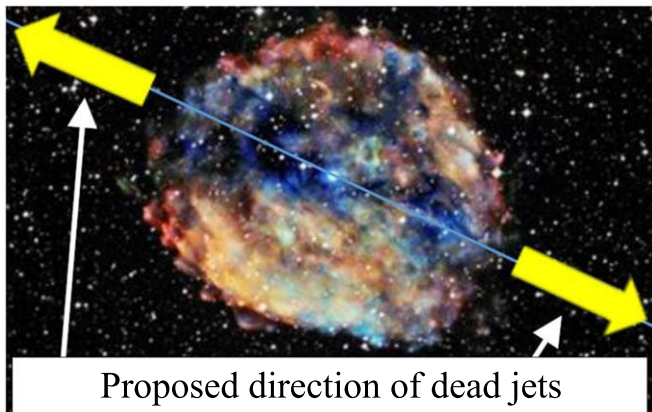


Figure 7. An X-ray image of RCW 103 in three energy bands (low=red, medium=green, highest=blue) combined with an optical image from the Digitized Sky Survey (image taken from the Chandra website based on Rea et al. 2016). The yellow arrows mark the original directions of the already dead jets as Bear et al. (2017) proposed.

addition there is a hollowed zone along the symmetry axis (yellow line). The sides of the symmetry axis display two opposite arcs on the outskirts of the ejecta which complicate the morphology. I classify it as a barrel-shaped SNR. No NS was found in this SNR, but its morphology and location in the Galaxy strongly suggest a CCSN origin (Gaensler et al. 1998).

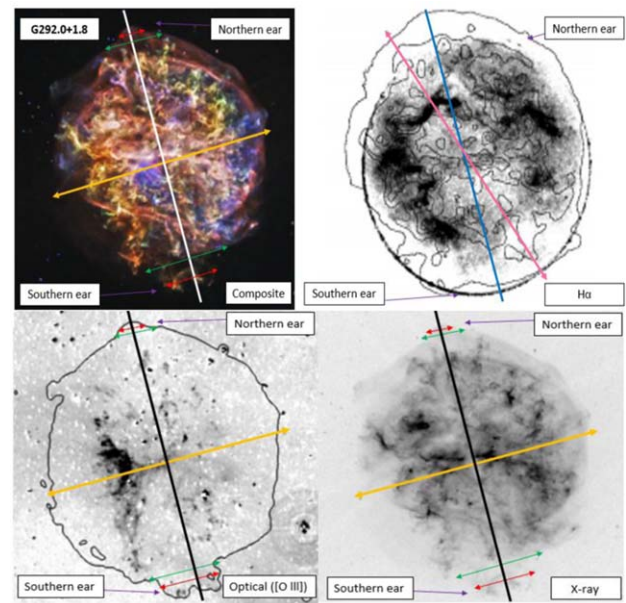


Figure 8. Images of the CCSNR G292.0+1.8 in various wavelengths with marks from Bear et al. (2017). In each image there is a line which connects the two opposite ears that Bear et al. (2017) define and analyze. On the $H\alpha$ image they also define the symmetry axis of the barrel-shaped morphology by the double-headed pink line. Upper-left panel: a composite X-ray image (Park et al. 2007) from the Chandra gallery where different lines represent different energy bands (for another X-ray image see Yang et al. 2014). Upper-right panel: zero velocity $H\alpha$ image taken from Ghavamian et al. (2005), which clearly reveals the barrel-shaped morphology. Lower-left panel: An optical ($[O III]$) image taken from Winkler & Long (2006) and reproduced by Ghavamian et al. (2012). Lower-right panel: A Chandra 0.3–8.0 keV X-ray image based on Park et al. (2007) and reproduced by Ghavamian et al. (2012).

If, as I argue in Section 3, the progenitor core was rapidly rotating it might have collapsed to a BH (see also Section 2.5).

Yu & Fang (2018) demonstrated by hydrodynamical simulations that jets with a total energy of $\simeq 10\%–15\%$ of the explosion energy can shape the morphology type of SNR G309.2-00.6.

The CCSNR G156.2+5.7 presents an interesting morphology. Its radio morphology with the polarization structure (magnetic fields) has a clear barrel-shaped morphology as the thorough observation and analysis by Xu et al. (2007) reveal. However, its $H\alpha$ (e.g., Gerardy & Fesen 2007) and X-ray (e.g., Pannuti & Allen 2004) images do not possess a barrel-shaped morphology (see comparison of images by Xu et al. 2007). It is a relatively old CCSNR, a few tens of thousands of years old (Katsuda et al. 2016). Therefore, most likely the interaction with the ISM played a major role in shaping its present morphology. For these reasons I do not classify it in this study.

2.5. Elongated SNRs

The fifth class is of an elongated morphology that only SNR W50 belongs to. However, there are large uncertainties because

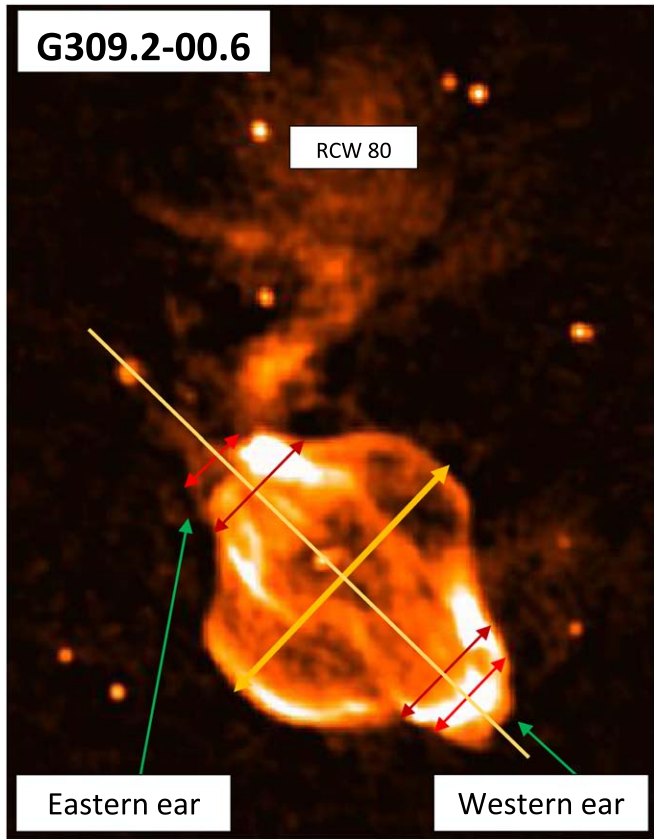


Figure 9. A radio image of SNR G309.2-00.6 from the site of the School of Physics, University of Sydney (posted as produced from Gaensler et al. 1998). Marks are from Grichener & Soker (2017). In the background is the emission nebula RCW 80.

of the shaping by the jets that its central binary system SS 433 launches and that are not related to the exploding jets. Specifically, the BH component of the binary systems launches these jets. In Figure, 10 I present its Low-Frequency Array (LOFAR) image that I take from Broderick et al. (2018) and its Very Large Array (VLA) radio continuum map from Dubner et al. (1998). I added to these two figures only what I identify as the boundaries between each ear and the main nebula by “kink” and “discontinuity.” Note that in two places the LOFAR image reveals a kink between the surface of the main nebula and the surface of the western ear, while the VLA image also displays a discontinuity between the two surfaces. These images show that although the two ears of W50 are connected to the main nebula with small variations between the main nebula and the ears, there is still a clear boundary between the nebula and the ears.

Ohmura et al. (2021) argue that the continuous jets from SS 433 formed the entire W50 nebula. The shocked material of the jets and of the ISM into which the jets propagate, i.e., the

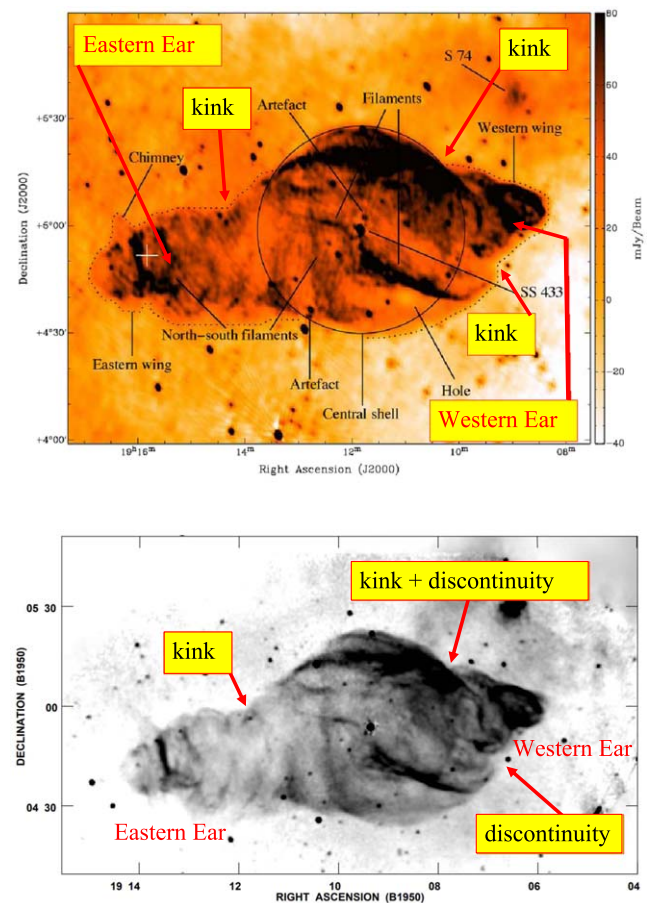


Figure 10. Upper panel: A LOFAR 140-MHz high-band continuum map of SNR W50 from Broderick et al. (2018). Color scale runs from -40 mJy/beam to 80 mJy/beam. Most marks are on the original image from Broderick et al. (2018). I added the marks of “kink” for the projected boundaries between the nebula and the ears. Lower panel: The SNR W50 in radio continuum at 1465 MHz as observed with the VLA (from Dubner et al. 1998). I added the marks of “kink” and “discontinuity” in the projected boundaries between the main nebula and the ears.

cocoons, formed the main nebula (the central part). The fronts of the jets form the ears. In their scenario SS 433 has been launching the jets for the last $\approx 10^5$ yr. The problem I find with their model is that their morphology does not reproduce clear boundaries between the main nebula and the two ears because the jets produce both the main nebula and the ears. Specifically, they do not reproduce the “kinks” and “discontinuities” that I mark on Figure 10. Goodall et al. (2011), on the other hand, do consider the W50 main nebula to be an SNR. They conduct hydrodynamical simulations where they launch jets that the BH in SS 433 launches into a spherical SNR. They obtain clear ears with clear boundaries from the main nebula. The problem I find

with the images that Goodall et al. (2011) obtain is that the ears largely differ from the main nebula, much more than observed.

The hydrodynamical simulation results of Ohmura et al. (2021) that the ears are basically part of the main nebula, more than observed in W50, and of Goodall et al. (2011), that the ears differ from the main nebula to a much larger degree than observed in W50, bring me to suggest an intermediate scenario. I take these results to imply that the ears were created during the jet-driven explosion process of W50 and were further shaped by the later jets that the system SS 433 has been launching.

In Section 3 I discuss the theoretical motivation to introduce the elongated class of SNRs.

3. The Possible Role of Core Rotation

In the JJEM there are two sources of angular momentum of the mass that the newly born NS accretes. This is true also in cases where the NS collapses to a BH. The first angular momentum source is the pre-collapse stochastic convection motion in the collapsing core that introduces angular momentum fluctuations with varying magnitudes and directions. The angular momentum fluctuations due to the core convective motion are amplified by instabilities in the zone between the newly born NS and the stalled shock at $\simeq 100$ km from the NS (Section 1). The other angular momentum source is the pre-collapse core rotation. It introduces an angular momentum component with a fixed direction. Its magnitude slowly increases with time as material from outer layers in the core are accreted.

In Soker (2023), I built a toy model to study the effects of these two angular momentum components on the direction of the jets. I used that toy model to offer an explanation to the $\simeq 2.5\text{--}5M_{\odot}$ mass gap between NSs and BHs in the frame of the JJEM. I assumed in that toy model that all specific angular momentum fluctuations of the random angular momentum component, after amplification by post-shock instabilities, have the same magnitude of j_f and have stochastic direction variations. I took the typical range of values to be $j_f \simeq 2 \times 10^{16} \text{ cm}^2 \text{ s}^{-1} \text{--} 5 \times 10^{16} \text{ cm}^2 \text{ s}^{-1}$. The pre-collapse core rotation introduces a fixed-direction specific angular momentum component of magnitude j_p . I found with the above toy model that when the core is slowly rotating, $j_p \lesssim 0.5j_f$, the jets are launched in all directions. According to the JJEM in this case, the jet feedback mechanism is efficient and the jets explode the core early-on, leaving an NS remnant (e.g., Shishkin & Soker 2022). When the pre-collapse core is rapidly rotating with $j_p \gtrsim j_f$, the NS does not launch jets in the equatorial plane of the pre-collapse rotating core (the plane perpendicular to \vec{j}_p) or its vicinity. The jets do not expel mass efficiently from the equatorial plane and accretion proceeds to form a BH. The BH might launch relativistic jets. Such jets might lead to new processes in the supernova that do not occur

when an NS is formed, e.g., neutrino emission as in choked gamma-ray bursts (as calculated by, e.g., Sahu & Zhang 2010; He et al. 2018; Fasano et al. 2021; Guetta et al. 2023).

The case with $j_p \gtrsim j_f$, therefore, both maintains a more or less fixed-axis direction of the jets and leaves a BH remnant. The fixed-axis jets form an elongated structure. This is the theoretical motivation behind the morphological class of elongated nebulae (Section 2.5), and in classifying W50, which has a BH in its central binary system, in this class. As discussed in Section 2.5, in the case of W50 the jets that the binary system SS 433 has been launching further shaped the ears.

In Soker (2023), I studied only the mass gap between NSs and BHs. I did not study the different cases of $j_p \lesssim j_f$ that leave an NS remnant. I now do that in relation to the first four classes in Table 1.

When the pre-collapse core rotation plays no role, namely $j_p \ll 0.1j_f$, the jets fully jitter at all jet-launching phases. Here I crudely estimate this range as $j_p \lesssim 0.01j_f$. The exact value should be determined in the future by highly demanding three-dimensional hydrodynamical simulations. In these cases the end period of the mass accretion process onto the newly born NS can be composed of several short, each lasting ≈ 0.01 s, jet-launching episodes that leave a point-symmetric structure in the outer regions of the ejecta. This is the case of SNR Vela (Figure 1; Section 2.1).

When the pre-collapse core rotation is somewhat larger, it might act to increase the probability of the jets' axis being close to the angular momentum axis of the pre-collapsing core, i.e., along \vec{j}_p . This might cause the last jet-launching episode to be somewhat longer and to form one dominant pair of opposite ears. The last jet-launching episode lasts for a relatively long time because of the following consideration. An accretion disk without a fresh supply of material lives for about the viscous timescale of the disk. This can be tens to hundreds of times the orbital period of the material. During the explosion process in the JJEM, newly accreted matter has a different angular momentum direction than the existing disk and it can destroy the disk. Namely, the freshly accreted material terminates the jets and starts a new jet-launching episode. The last accretion episode in the JJEM has no fresh supply of material. The accretion disk can live for the viscous timescale. For an NS of mass $M_{\text{NS}} = 1.4M_{\odot}$ and an accretion disk at $r = 30$ km, the orbital period of the material is 0.0024 s. The viscous timescale might be $\approx 0.1\text{--}1$ s. This is a relatively long time (as a regular jet-launching episode lasts for $\approx 0.01\text{--}0.1$ s) during which the outer core expands and the final material of these last jets shapes the ears in the expanding core and envelope. I therefore suggest that for the range of $j_p \approx 0.01j_f\text{--}0.1j_f$ (admittedly this range is a crude estimate), the last jets form a prominent pair of ears, e.g., the one-pair morphology. The final accretion disk

might precess due to perturbations by accreted parcels of material, leading to an S-shaped morphology.

When the pre-collapse core angular momentum is larger, but not as to form a BH, the last jet-launching episode might be longer and more powerful. The jets can clear the central zone around the core angular momentum axis and form a barrel-like morphology. I crudely take this range to be $j_p \approx 0.1j_f - 0.3j_f$.

These ranges are crude estimates within the frame of the toy model. The situation is more complicated as the specific angular momentum fluctuations do not have a constant magnitude as the toy model assumes.

I note that the final angular momentum of the NS does not relate monotonically to the pre-collapse core rotation. The reason is that, in the JJEM, the jets of each jet-launching episode carry most of the angular momentum of the accretion disk that launches the jets. In the case of a rapid pre-collapse rotation, there might be one long-lived jet-launching episode with a fixed jets' axis. However, in that case the magnetic fields in the NS and in the accretion disk might very efficiently slow down the NS by coupling the NS to outer disk radii where angular velocity is much slower. Furthermore, after accretion ceases, rapidly rotating NSs substantially slow-down by blowing winds (e.g., Prasanna et al. 2022) in the propeller mechanism (e.g., Ott et al. 2006). Therefore, in most, but not in all, cases the JJEM mechanism expects a spin-period of tens of milliseconds shortly after explosion (e.g., Gofman & Soker 2020).

The main point to take from this section is that in the frame of the JJEM the pre-collapse core rotation, or more specifically the ratio j_p/j_f , is the main parameter that determines the outer large-scale morphology of CCSNRs. Other factors are the nonlinear instabilities that occur during the explosion, the possible presence of a binary companion, circumstellar material into which the ejecta expand (e.g., Velázquez et al. 2023), the energy of the explosion and the ejecta mass, and the ISM (in particular with a strong magnetic field, e.g., Wu & Zhang 2019; Velázquez et al. 2023).

4. Summary

I classified 14 CCSNRs into five classes according to morphological features that late jets in the explosion process might form (Table 1). According to the JJEM, after the early jets explode the core, the late jets that interact with the already expanding star might leave imprints on the ejecta, and outer and inner regions (e.g., Grichener & Soker 2017; Bear et al. 2017).

Late jittering jets where more than one pair of jets leave imprints on the ejecta shape a point-symmetric morphology (Figure 1). I attribute this type of shaping to cases where the pre-collapse core rotation is extremely slow. Namely, the specific angular momentum in the relevant layer of the core due to its rotation is much smaller than the typical magnitude

of the specific angular momentum fluctuations due to pre-collapse core convection. Based on earlier results (Soker 2023), I crudely estimate this range to be $j_p \lesssim 0.01j_f$, as I list in the second row of Table 1 and discuss in Section 3.

More rapidly rotating cores might force the last pair of jets to be long-lived and shape one pair of jet-inflated ears that dominates the morphology (Figures 2, 3, 4, and 5). The accretion disk might precess, therefore leading to an S-shaped morphology (Figure 6). I crudely estimate that these cases occur when $j_p \approx 0.01j_f - 0.1j_f$. Even more rapidly rotating pre-collapse cores, which I crudely estimate to have $j_p \approx 0.1j_f - 0.3j_f$, might clear the region along the axis of the pre-collapse core rotation and form a barrel-shaped morphology (Figures 7, 8, and 9).

The most uncertain class of this study is the elongated morphology which includes only SNR W50 which has a binary system that launches jets (Figure 10). I argued in Section 2.5 that both the exploding jets and the jets that the BH in the binary system launches have shaped the ears of W50. This class occurs when $j_p \gtrsim j_f$ and the jets maintain a more or less constant axis. The jets are inefficient in expelling mass from the equatorial plane and the long-lasting accretion process turns the NS into a BH.

Although I take the ratio j_p/j_f to be the main factor that determines the CCSNR morphology, it is definitely not the only one. Other processes might occur, in particular large-scale instabilities during the explosion process. Then there are possibilities of the presence of a binary companion, a circumstellar material into which the ejecta expand and the ISM. For these, it is expected that opposite structural features, like opposite ears and arcs, will not be equal to each other.

Although the morphologies of all 14 CCSNRs have been analyzed in the past (see figure captions), this study reports two new results. The first is the classification of CCSNRs to five classes based on jet-shaped morphological features. The second new result is the attribution of the morphological classes to the degree of pre-collapse core rotation as the main (but not sole) factor that determines the morphology class of a CCSNR.

I note that by the same physics by which the jets shape CCSNRs, they can account for non-zero polarization in CCSNe, e.g., as Nagao et al. (2023) report recently. Nagao et al. (2023) find that the explosion asphericity is proportional to the explosion energy and note that jets might account for that. I add here that the JJEM can naturally account for this finding. I take their results to support the JJEM.

Overall, this study adds some support to the argument that jets, in particular jittering jets (the JJEM), explode most, or even all, CCSNe. The complicated nature of the explosion process, and the highly demanding numerical simulations that are required to simulate the JJEM, force progress to be made in small steps.

Acknowledgments

I thank Aldana Grichener and Dima Shishkin for helpful discussions and comments. I thank an anonymous referee for helpful comments. This research was supported by a grant from the Israel Science Foundation (769/20).

ORCID iDs

Noam Soker  <https://orcid.org/0000-0003-0375-8987>

References

- Aloy, M. A., Muller, E., Ibanez, J. M., Marti, J. M., & MacFadyen, A. 2000, *ApJ*, **531**, L119
- Antoni, A., & Quataert, E. 2023, *MNRAS*, **525**, 1229
- Aschenbach, B., Egger, R., & Trümper, J. 1995, *Natur*, **373**, 587
- Bear, E., Grichener, A., & Soker, N. 2017, *MNRAS*, **472**, 1770
- Bethe, H. A., & Wilson, J. R. 1985, *ApJ*, **295**, 14
- Boccioli, L., Mathews, G. J., Suh, I.-S., & O'Connor, E. P. 2022, *ApJ*, **926**, 147
- Broderick, J. W., Fender, R. P., Miller-Jones, J. C. A., et al. 2018, *MNRAS*, **475**, 5360
- Bromberg, O., & Tchekhovskoy, A. 2016, *MNRAS*, **456**, 1739
- Burrows, A., & Vartanyan, D. 2021, *Natur*, **589**, 29
- Drew, J. E., Greimel, R., Irwin, M. J., et al. 2005, *MNRAS*, **362**, 753
- Dubner, G. M., Holdaway, M., Goss, W. M., & Mirabel, I. F. 1998, *AJ*, **116**, 1842
- Fasano, M., Celli, S., Guetta, D., et al. 2021, *JCAP*, **2021**, 044
- Fryer, C. L., Olejak, A., & Belczynski, K. 2022, *ApJ*, **931**, 94
- Fujibayashi, S., Takahashi, K., Sekiguchi, Y., & Shibata, M. 2021, *ApJ*, **919**, 80
- Gaensler, B. M., Green, A. J., & Manchester, R. N. 1998, *MNRAS*, **299**, 812
- García, F., Suárez, A. E., Miceli, M., et al. 2017, *A&A*, **604**, L5
- Gerardy, C. L., & Fesen, R. A. 2007, *MNRAS*, **376**, 929
- Ghavamian, P., Hughes, J. P., & Williams, T. B. 2005, *ApJ*, **635**, 365
- Ghavamian, P., Long, K. S., Blair, W. P., et al. 2012, *ApJ*, **750**, 39
- Gilkis, A., & Soker, N. 2015, *ApJ*, **806**, 28
- Gofman, R. A., & Soker, N. 2020, *MNRAS*, **494**, 5902
- Goodall, P. T., Alouani-Bibi, F., & Blundell, K. M. 2011, *MNRAS*, **414**, 2838
- Gottlieb, O., Liska, M., Tchekhovskoy, A., et al. 2022, *ApJL*, **933**, L9
- Grichener, A., & Soker, N. 2017, *MNRAS*, **468**, 1226
- Grimmett, J. J., Müller, B., Heger, A., Banerjee, P., & Obergaulinger, M. 2021, *MNRAS*, **501**, 2764
- Guetta, D., Langella, A., Gagliardini, S., & Della Valle, M. 2023, *ApJL*, **955**, L9
- Guetta, D., Rahin, R., Bartos, I., & Della Valle, M. 2020, *MNRAS*, **492**, 843
- Gvaramadzé, V. V. 2006, *A&A*, **454**, 239
- He, H.-N., Kusenko, A., Nagataki, S., Fan, Y.-Z., & Wei, D.-M. 2018, *ApJ*, **856**, 119
- Heger, A., Fryer, C. L., Woosley, S. E., Langer, N., & Hartmann, D. H. 2003, *ApJ*, **591**, 288
- Hester, J. J. 2008, *ARA&A*, **46**, 127
- Hwang, U., Laming, J. M., Badenes, C., et al. 2004, *ApJL*, **615**, L117
- Janka, H.-T. 2012, *ARNPS*, **62**, 407
- Katsuda, S., Tanaka, M., Morokuma, T., Fesen, R., & Milisavljevic, D. 2016, *ApJ*, **826**, 108
- Katsuda, S., & Tsunemi, H. 2005, *PASJ*, **57**, 621
- Katsuda, S., & Tsunemi, H. 2006, *ApJ*, **642**, 917
- Khokhlov, A. M., Höflich, P. A., Oran, E. S., et al. 1999, *ApJL*, **524**, L107
- Larsson, J., Sollerman, J., Lyman, J. D., et al. 2021, *ApJ*, **922**, 265
- López-Cámara, D., Morsony, B. J., Begelman, M. C., & Lazzati, D. 2013, *ApJ*, **767**, 19
- Lu, C.-Y., Yan, J.-W., Wen, L., & Fang, J. 2021, *RAA*, **21**, 033
- MacFadyen, A. I., Woosley, S. E., & Heger, A. 2001, *ApJ*, **550**, 410
- Maeda, K., Moriya, T., Kawabata, K., et al. 2012, *MmSAI*, **83**, 264
- Miceli, M., Bocchino, F., & Reale, F. 2008, *ApJ*, **676**, 1064
- Morse, J. A., Smith, N., Blair, W. P., et al. 2006, *ApJ*, **644**, 188
- Müller, B., Tauris, T. M., Heger, A., et al. 2019, *MNRAS*, **484**, 3307
- Nagao, T., Patat, F., Cikota, A., et al. 2023, arXiv:2308.00996
- Nakamura, K., Takiwaki, T., & Kotake, K. 2022, *MNRAS*, **514**, 3941
- Nishimura, N., Sawai, H., Takiwaki, T., Yamada, S., & Thielemann, F.-K. 2017, *ApJL*, **836**, L21
- Nordhaus, J., Brandt, T. D., Burrows, A., & Almgren, A. 2012, *MNRAS*, **423**, 1805
- Obergaulinger, M., & Reichert, M. 2023, arXiv:2303.12458
- Ohmura, T., Ono, K., Sakemi, H., et al. 2021, *ApJ*, **910**, 149
- Olejak, A., Fryer, C. L., Belczynski, K., & Baibhav, V. 2022, *MNRAS*, **516**, 2252
- Ott, C. D., Burrows, A., Thompson, T. A., Livne, E., & Walder, R. 2006, *ApJS*, **164**, 130
- Pannuti, T. G., & Allen, G. E. 2004, *AdSpR*, **33**, 434
- Papish, O., & Soker, N. 2011, *MNRAS*, **416**, 1697
- Papish, O., & Soker, N. 2014a, *MNRAS*, **438**, 1027
- Papish, O., & Soker, N. 2014b, *MNRAS*, **443**, 664
- Park, S., Hughes, J. P., Slane, P. O., et al. 2003, *ApJL*, **592**, L41
- Park, S., Hughes, J. P., Slane, P. O., et al. 2007, *ApJL*, **670**, L121
- Perley, D. A., Sollerman, J., Schulze, S., et al. 2021, arXiv:2111.12110
- Prasanna, T., Coleman, M. S. B., Raives, M. J., & Thompson, T. A. 2022, *MNRAS*, **517**, 3008
- Quataert, E., Lecoanet, D., & Coughlin, E. R. 2019, *MNRAS*, **485**, L83
- Rea, N., Borghese, A., Esposito, P., et al. 2016, *ApJL*, **828**, L13
- Ren, J.-J., Liu, X.-W., Chen, B.-Q., et al. 2018, *RAA*, **18**, 111
- Reynoso, E. M., Cichowolski, S., & Walsh, A. J. 2017, *MNRAS*, **464**, 3029
- Reynoso, E. M., Johnston, S., Green, A. J., & Koribalski, B. S. 2006, *MNRAS*, **369**, 416
- Reynoso, E. M., & Walsh, A. J. 2015, *MNRAS*, **451**, 3044
- Sahai, R. 2000, *ApJL*, **537**, L43
- Sahai, R., & Trauger, J. T. 1998, *AJ*, **116**, 1357
- Sahu, S., & Zhang, B. 2010, *RAA*, **10**, 943
- Sankrit, R., Blair, W. P., & Raymond, J. C. 2003, *ApJ*, **589**, 242
- Sapienza, V., Miceli, M., Peres, G., et al. 2021, *A&A*, **649**, A56
- Schreier, R., & Soker, N. 2016, *RAA*, **16**, 70
- Seward, F. D., Tucker, W. H., & Fesen, R. A. 2006, *ApJ*, **652**, 1277
- Shelton, R., Kuntz, K., & Petre, R. 2004, *ApJ*, **611**, 906
- Shishkin, D., & Soker, N. 2021, *MNRAS*, **508**, L43
- Shishkin, D., & Soker, N. 2022, *MNRAS*, **513**, 4224
- Slane, P., Helfand, D., Swaluw, E., & Murray, S. 2004, *ApJ*, **616**, 403
- Soker, N. 2010, *MNRAS*, **401**, 2793
- Soker, N. 2019, *RAA*, **19**, 095
- Soker, N. 2020, *RAA*, **20**, 024
- Soker, N. 2022a, *RAA*, **22**, 035019
- Soker, N. 2022b, *RAA*, **22**, 095007
- Soker, N. 2022c, *RAA*, **22**, 122003
- Soker, N. 2023, *RAA*, **23**, 095020
- Urrutia, G., De Colle, F., & López-Cámara, D. 2023, *MNRAS*, **518**, 5145
- Vartanyan, D., Coleman, M. S. B., & Burrows, A. 2022, *MNRAS*, **510**, 4689
- Velázquez, P. F., Meyer, D. M.-A., Chiotellis, A., et al. 2023, *MNRAS*, **519**, 5358
- Wang, S.-Q., Wang, L.-J., & Dai, Z.-G. 2019, *RAA*, **19**, 063
- Winkler, P. F., & Long, K. S. 2006, *AJ*, **132**, 360
- Wongwantharat, A., Janka, H.-T., Müller, E., Pllumbi, E., & Wanajo, S. 2017, *ApJ*, **842**, 13
- Wongwantharat, A., Müller, E., & Janka, H.-T. 2015, *A&A*, **577**, A48
- Wu, D., & Zhang, M.-F. 2019, *RAA*, **19**, 124
- Xiao, L., Zhu, M., Sun, X.-H., Jiang, P., & Sun, C. 2022, *RAA*, **22**, 035003
- Xu, J. W., Han, J. L., Sun, X. H., et al. 2007, *A&A*, **470**, 969
- Yang, X.-J., Liu, X.-Q., Li, S.-Y., & Lu, F.-J. 2014, *RAA*, **14**, 1279
- Yu, H., & Fang, J. 2018, *RAA*, **18**, 117